# Log interpretation of marly chalk, the Lower Cretaceous Valdemar Field, Danish North Sea: Application of iso-frame and pseudo water film concepts

*Ida L. Fabricius and Casper Olsen, Technical University of Denmark, Lyngby*
*Manika Prasad, Colorado School of Mines, Golden, USA*

Low-permeability marly chalk reservoirs are challenging to develop. Among the difficulties is interpretation of fluid distribution, due to the dominance of capillary forces, and a lack of cementation that might result in reservoir compaction upon draw down.

For evaluation of wells, the choice of well logs depends on the purpose of interpretation.

Standard petrophysical interpretation has the aim of establishing porosity and fluid saturation, and the broader aim of establishing lithological compostion, porosity, water saturation, and (if possible) to predict permeability. Logs used for this purpose include resistivity logs of different depths of investigation, the density log based on gamma ray attenuation, the neutron porosity log, and the natural background gamma ray log.

Rock physics interpretation establishes the elastic properties of the formation. It is commonly based on interpreted logs of porosity, lithological composition, and water saturation in combination with bulk density and sonic logs. Bulk density, $\rho_b$, is derived from density logs, and sonic logs measure the P-wave velocity, $V_P$, and preferably also the shear-wave velocity, $V_S$. The elastic properties may be expressed as elastic moduli describing the stress required for elastic deformation. Elastic moduli include: the P-wave modulus, M, corresponding to uniaxial confined deformation, $M = V_P^2\rho_b$; the shear modulus, G, corresponding to shear deformation: $G = V_S^2\rho_b$; and the bulk modulus, K, corresponding to hydrostatic deformation: $K = M - \frac{4}{3} G$.

We demonstrate how the sonic log can be integrated in the petrophysical well log interpretation via the iso-frame concept (Fabricius 2003) to obtain a measure of formation stiffness. We also show how we may locate sealing intervals and discuss hydraulic equilibrium via the pseudo water film thickness concept (Larsen and Fabricius, 2004).

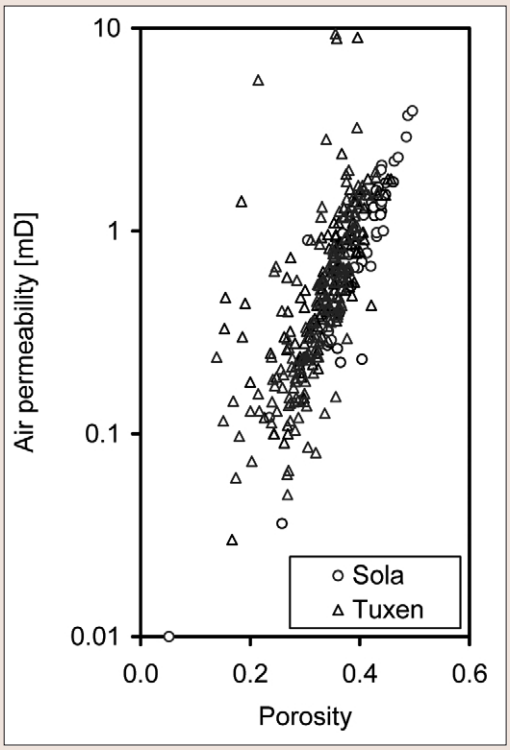


***Figure 1.*** *Air permeability versus He porosity. Although data from Tuxen are more scattered, data from Sola Formation and Tuxen Formation fall roughly along the same trend.*

***Table 1.*** *Stratigraphy of North Jens-1 well (Jakobsen et al., 2004)*

| | | | |
|---|---|---|---|
| Cenomanian | Chalk Group | | |
| Late Albian | Cromer Knoll Group | Rødby Formation | Pelagic chalks and marlstones |
| Early Albian | | Sola Formation, including Fisch Schiefer Bed | Claystone |
| Aptian-Barremian | | | Chalk and marly chalk interbedded with marlstones |
| Barremian | | | |
| | | Tuxen Formation, including Munk Marl Bed | Chalk and marly chalk |
| | | | Marlstone |
| Barremian-Hauterivian | | | Chalk, marly chalk |
| Hauterivian-Valanginian Ryazanian | | Åsgard Formation | Calcareous claystones |

**Iso-frame modeling and pseudowater film model.** The iso-frame concept is based on effective medium theory, applying the modified Hashin Strikman model of Nur et al. (1998). For a given porosity, an elastic modulus for a sediment falls within two bounds—a lower bound corresponding to all solids in suspension (iso-frame value = 0) and an upper bound corresponding to all solids in the frame supporting the sediment (iso-frame value = 1). In the iso-frame model, a given porosity and elastic modulus correspond to an iso-frame value that describes the extent of the solid that may be regarded as in the solid frame; the remaining solid is visualized as being in suspension. Iso-frame modeling requires a normal sonic log giving $V_P$; shear log data are not required.

In the pseudo water film model, a given water saturation is recalculated to equivalent water film thickness on the pore wall. For pure chalk, the area of the pore wall may be calculated from Kozeny's equation, when core data on poros-

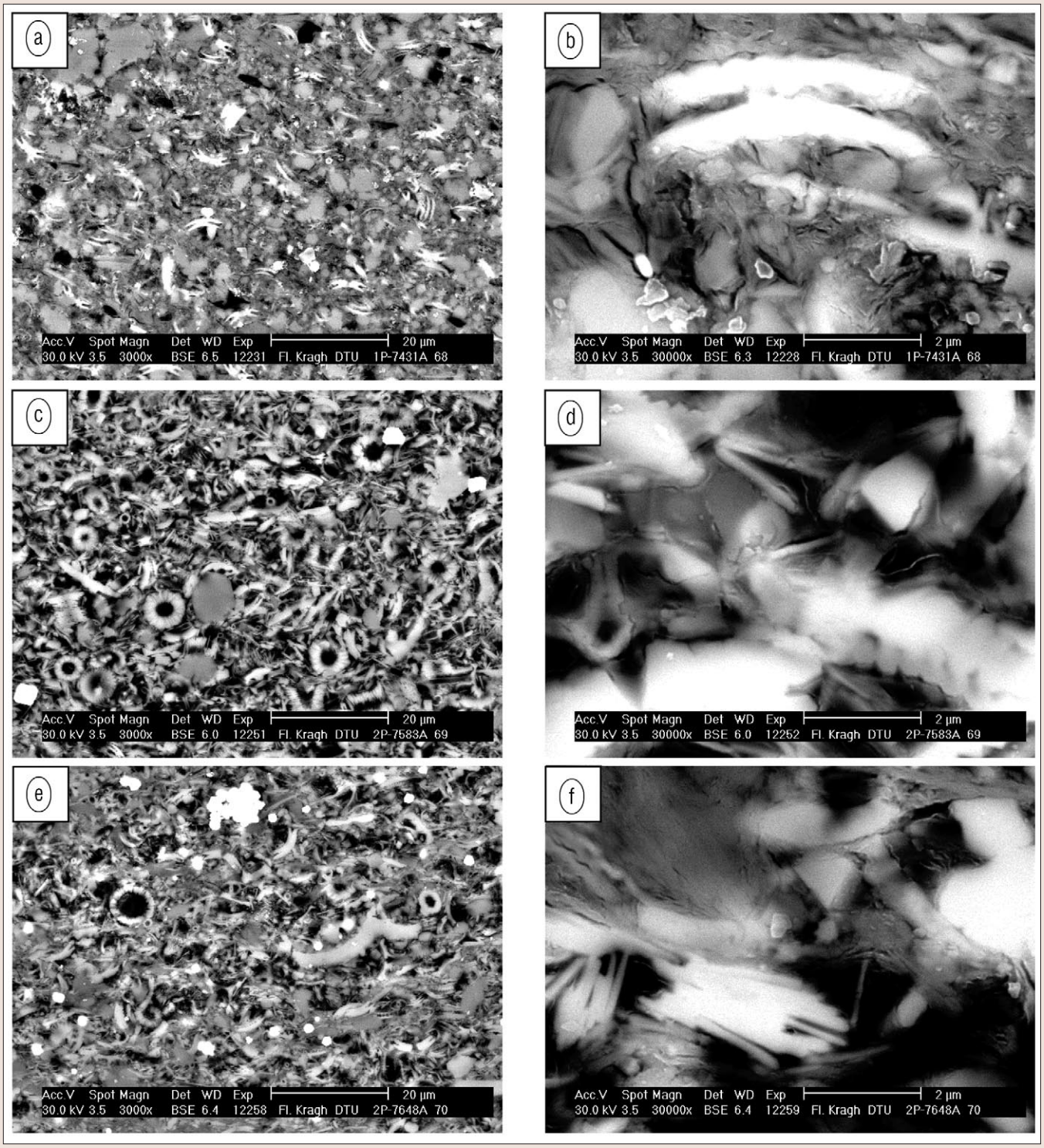


***Figure 2.*** *Backscatter electron micrographs of samples from Valdemar wells. Gray silicates and light gray calcitic micro- and nannofossils support the frame to varying extent. (a and b) Valdamar-1P, Sola Formation, 7205 ft ss. Carbonate content 13.2%, porosity 17.5%, permeability below 0.02 mD. Both silicates and coccoliths are frame supporting. (c and d) Valdemar-2P, Tuxen Formation, 7322 ft ss. Carbonate content 79.8%, porosity 37.9%, permeability 0.7 mD. The solid particles are only partly frame-supporting. (e and f) Valdemar-2P, Tuxen Formation, 7383 ft ss. Carbonate content 60.8%, porosity 26.7%, permeability 0.1 mD. The solid particles are only partly frame-supporting. X-ray diffraction data indicated that the silicates are mainly kaolinite with minor illite and quartz.*

ity and permeability are known. In this study, the pore area (specific surface) was obtained from the natural gamma log calibrated with core data. For a given lithology, the thickness of the pseudo water film is controlled by the capillary pressure, so in the present case the water film data are calibrated with data on capillary pressure from core samples. The capillary pressure is controlled by the distance to the free water level (e.g., Aguilera, 2002). Above the zone of transitional water saturation, the gradient of the water film thickness may be described by a straight line and the location of the free water level may be predicted.

We demonstrate the use of the two concepts in the interpretation of log and core data from wells in the marly chalk of Valdemar Field, Danish North Sea, where silicate content and low permeability make interpretation of reservoir pressure difficult and well bore stability is a concern.

**Table 2.** *Data used in present study (Maersk Oil and Gas AS, GEUS, and "PRIORITY Database")*

| Well | Year drilled | Mud type | Wireline formation-tester | Hole size, resistivity log | Conventional core analysis | Special core analysis | Data added in this study |
|---|---|---|---|---|---|---|---|
| Bo-1 | 1977 | Water-based Mud weight 14.8 ppg | | c. 12.5" LLD 7500 ft tvd c. 9.5" ILD | He-porosity, gas-perm., grain density | | |
| NJens-1 | 1986 | Water-based Mud weight 14.0 ppg | + | c. 12.5" LLD | He-porosity, gas-perm., grain density | Ins. residue capillary curves (Hg) | |
| Val-1P | 1989 | Oil-based Mud weight 13.1 ppg | + | c. 12.5" ILD | He-porosity, gas-perm., grain density | Ins. residue capillary curves (Hg) | |
| Val-2P | 1990 | Oil-based Mud weight 13.8 ppg | | c. 12.5" ILD | He-porosity, gas-perm., grain density | Ins. residue capillary curves (Hg) | |
| Val-3H | 1994 | Water-based, high KCl | + | | | Resistivity | BET, XRD ins.residue |

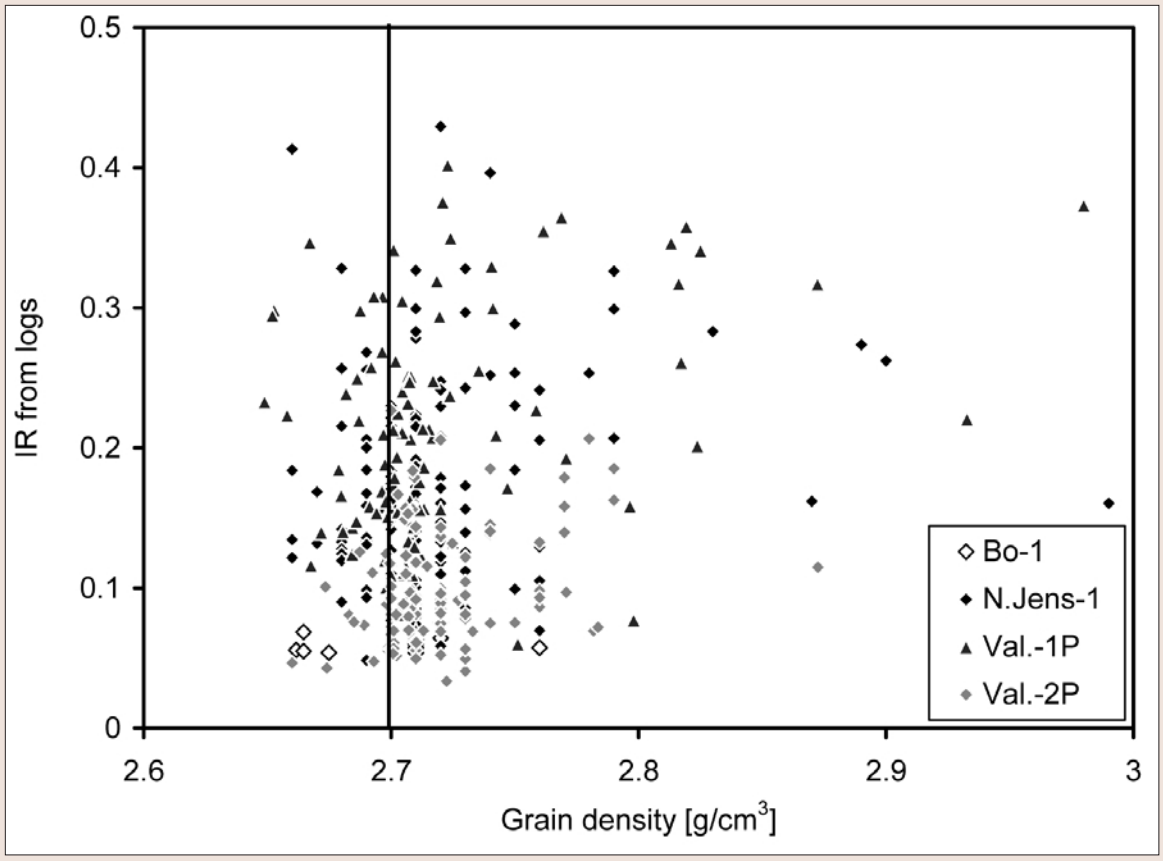


*Figure 3. Grain density from He porosimetry compared to bulk IR content from log analysis at (depth-matched) corresponding depth. GR data were recalculated to bulk IR as shown in Figure 5. Because we find no obvious relationship between grain density and IR from logs, we use a constant grain density of 2.7 g/cm$^3$ for the log analysis.*

**Valdemar Field.** This field is a low relief structure in the Cromer Knoll Group, Danish North Sea. The reservoir intervals are in Barremian-Aptian interlayered chalks and marly chalks of Tuxen and Sola formations, sealed by claystone in the upper part of the Sola (Table 1). The reservoir intervals may have high porosity, but permeability tends to be low (Figure 1). Jakobsen et al. (2004) found that the noncalcite component in the marly chalk is predominantly kaolinite with some quartz and illite. They found a negative correlation between porosity and noncarbonates, indicating that the silicates are mainly pore filling. BSE imaging indicates that this is the case in most but not all intervals. In some intervals the silicates are load-bearing (Figure 2). Jakobsen et al. also found a higher content of noncarbonates for a given porosity in Sola Formation than in Tuxen.

In the present study we include core and logging data from two exploration wells (Bo-1 and NJens-1) and from two pilot holes (Valdemar-1P and Valdemar-2P). The exploration wells were drilled with water-based mud. The two pilot holes were drilled with oil-based mud. In addition we use wire-line formation tester and core data from the build section of a horizontal well (Valdemar-3H).

**Procedure.** Basic log interpretation included quality control,

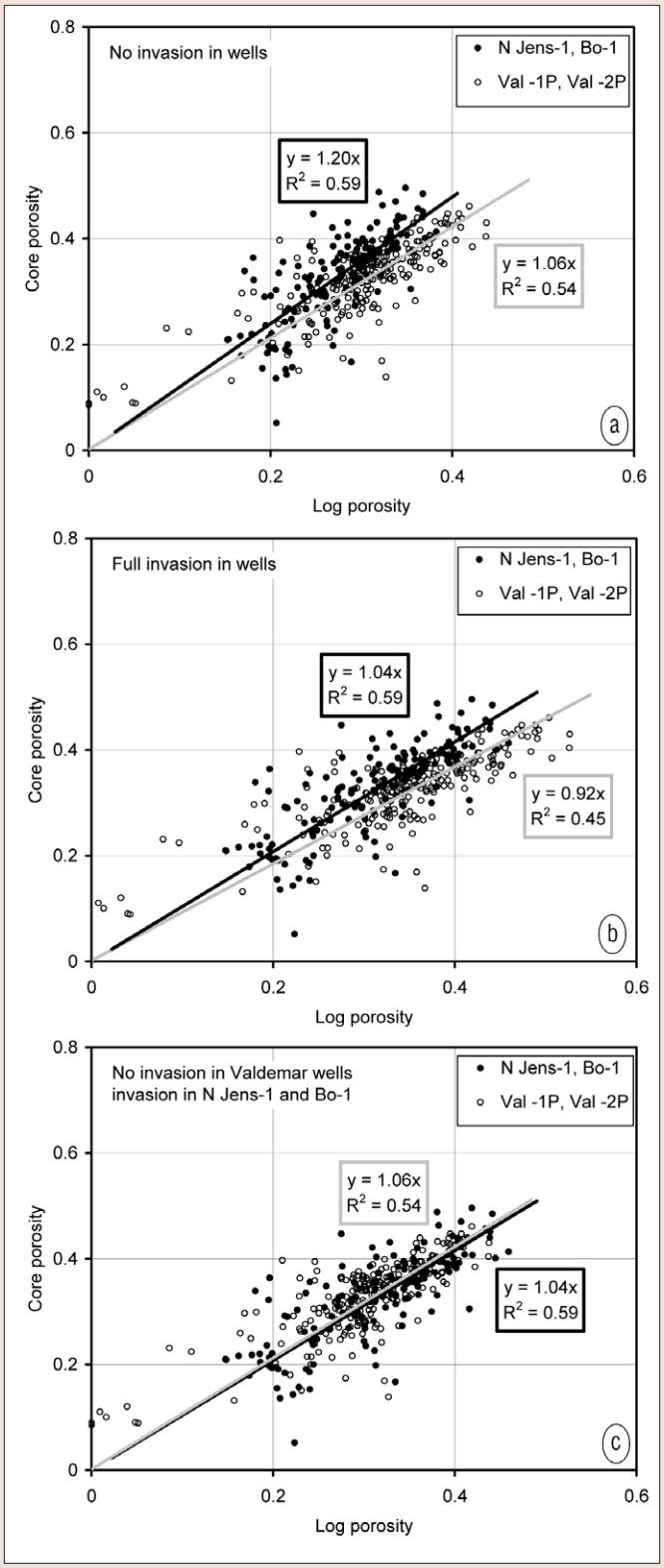


***Figure 4.*** *Comparison of porosity as calculated from density log and by core analysis (He). (a) The log porosity (and water saturation) is calculated by iteration from density and deep restivity log under assumption of no water invasion. The log-based prediction of porosity seem unrealistically low for exploration wells NJens-1 and Bo-1. (b) The log porosity is calculated from density log and a mud filtrate density of 1.03 g/cm$^3$ (Table 3), under assumption of full invasion. The log-based prediction of porosity seems unrealistically high for the holes drilled with oil-based mud (Val-1P and Val-2P). (c) When we assume full water invasion in NJens-1 and Bo-1 and no net invasion in Val-1P and Val-2P, the core data and log-data are related by the same equation for all wells, indicating a porosity rebound of 5% on core retrieval.*

determination of porosity, content of noncarbonates, and water saturation. All logs were checked for data quality, spurious data were deleted, and one deep resistivity, $R_t$-log was selected for each well (Table 2).

Porosity was calculated from the density log under assumption of full or absent invasion and by assuming that grain density = 2.7 g/cm$^3$. A constant grain density independent of content of noncarbonates is justified by core data (Figure 3), and seems reasonable because of the dominance of kaolinite among the silicates. In exploration wells Bo-1 and NJens-1, comparison of porosity calculated from the density log with core porosity indicates practically full invasion and a porosity rebound of 4%; however, the porosity data from two pilot holes, Val-1P, and Val-2P, correspond to a situation with close to no invasion and a porosity rebound of 6% (Figure 4). On this basis the porosity rebound is assumed near 5% for all wells.

Content of noncarbonates in solid phase, IR (mass/solid mass), was calculated from the natural gamma ray (GR), and density log, calibrated to core data. The density must be taken into account because GR logging data are derived from fluid-saturated bulk sediment and IR in the laboratory is determined on dry samples. The radiation per bulk volume should thus be proportional to the insoluble residue per (dry) bulk volume:

$$GR\ \rho_b \sim IR\ \rho_g\ (1-\phi/1.05) \qquad (1)$$

where $\rho_b$ and $\rho_g$ are, respectively, bulk and grain densities, and $\phi/1.05$ is core porosity corrected for rebound. This approach involves a simplification because the gamma ray intensity may not be equally related to silicate content in all logged layers. Indeed, spectral gamma logs from some Valdemar wells show intervals of high U radiation without an equivalently high silicate content.

Because the GR log also depends on hole size and mud properties, calibration is necessary. The volume of insoluble residue per fluid-saturated bulk volume becomes:

$$IR_{bv} = (GR\ \rho_b\ a - b)/\rho_g \qquad (2)$$

where a and b for the present wells are assessed to be 0.008/API and 0.16 g/cm$^3$, respectively, (Figure 5); and IR becomes

$$IR = IR_{bv}\ \rho_g/\rho_b = (GR\ \rho_b\ a - b)/\rho_b \qquad (3)$$

Determining water saturation in clay-bearing formations involves a choice of model. We have chosen the dual water method of Clavier et al. (1977), but this choice does not influence the use of the concepts of iso-frame value or pseudo water film thickness. Water saturation was calculated by different strategies, the choice depending on whether full or no invasion is assumed. For the oil-based pilot wells, no invasion was assumed, and water saturations and porosity were calculated by iteration from $\rho_b$, $R_t$, and GR. For the water-based exploration wells with full invasion assumed, water saturation was calculated on the basis of porosity from density log as well as $R_t$, and GR. The detailed procedure for calculating porosity and water saturation is given in Appendix 1.

During log interpretation, prediction of permeability may be attempted, typically from porosity. In the present study we combine porosity and natural gamma radiation. From gamma ray logs we predict the specific surface, A, and according to Mortensen et al. (1998) permeability, $k$, of a

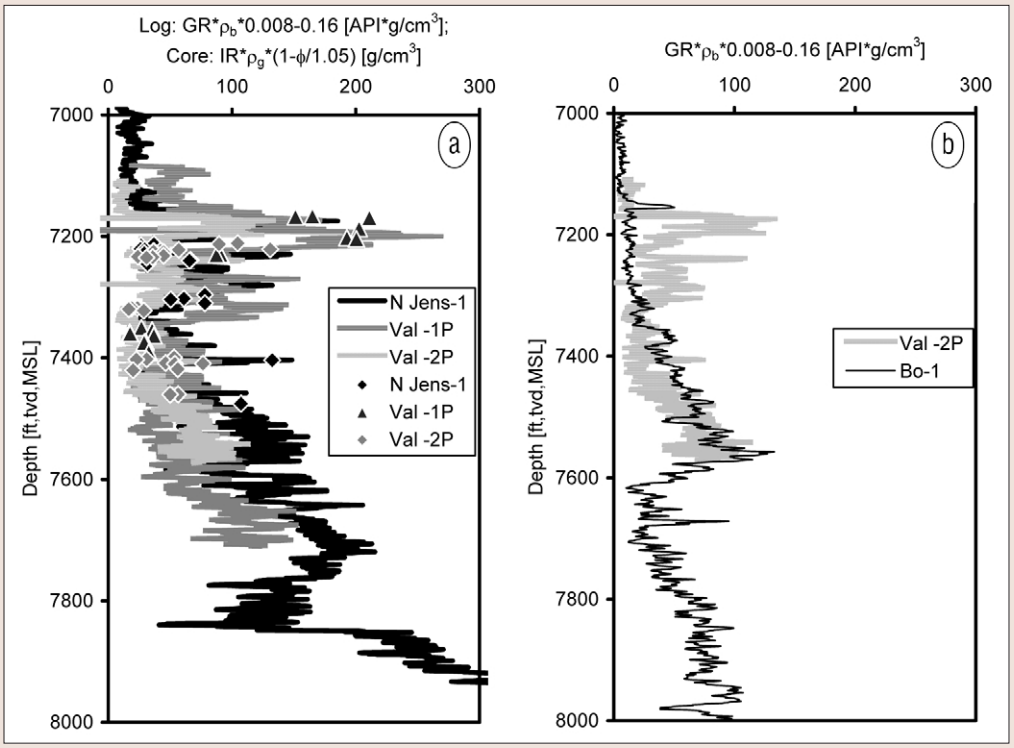


*Figure 5. Natural GR logs from studied wells. The wells have roughly comparable hole size and mud weight (Table 2). (a) Wells where core insoluble residue (IR) data are available. In order to match GR log data, core data are recalculated to IR per bulk volume. GR log data are normalized to bulk volume by multiplication by bulk density and shifted so as to match core data. (b) For Bo-1, where core data are not available, GR values are shifted in the same way as in other wells.*

homogeneous chalk may be calculated from Kozeny's equation:

$$k = c\frac{\phi^3}{A_{hom}^2} \quad (4)$$

where c is Kozeny's constant, which should be around 0.22 in the present porosity range. $A_{hom}$ is specific surface with respect to bulk volume in a homogeneous system. Specific surface with respect to bulk volume, $A_{bv}$, in any system is

$$A_{bv} = A\,\rho_g\,(1-\phi) \quad (5)$$

The marly chalk of the studied formations can hardly be expected to be homogeneous, so we should not be able to use Kozeny's equation directly. Thus, to find a way to predict permeability from logging data we proceed as follows: For the core samples, data on A, He-permeability, $k_a$, and $\phi$ are available, and from A we derive $A_{bv}$ from equation 5. $A_{hom}$ may be derived from $\phi$ and $k_a$ by first Klinkenberg-correcting $k_a$ (in mD) according to an empirical formula from Mortensen et al. and recalculating to SI units ($m^2$):

$$k = 0.52\,k_a^{1.083}\,0.9869\,10^{-15}$$

or rearranged:

$$k_a = \left(\frac{k}{0.52\cdot 0.98969\cdot 10^{-15}}\right)^{1/1.083} \quad (6)$$

$A_{hom}$ may now be calculated from equation 4. Comparison of $A_{hom}$ and $A_{bv}$ (in 1/μm) show that they are related by the equation (Figure 6):

$$A_{hom} = 0.95\,A_{bv}^{0.74} \quad (7)$$

We may thus predict permeability from logging data on $\phi$ and IR, by first calculating A from equation A5; next assuming $\rho_g = 2.7$ g/cm$^3$ and deriving $A_{bv}$ from equation 5; calculating $A_{hom}$ from equation 7; calculating $k$ from equation 4; and finally deriving $k_a$ by the rearranged equation 6.

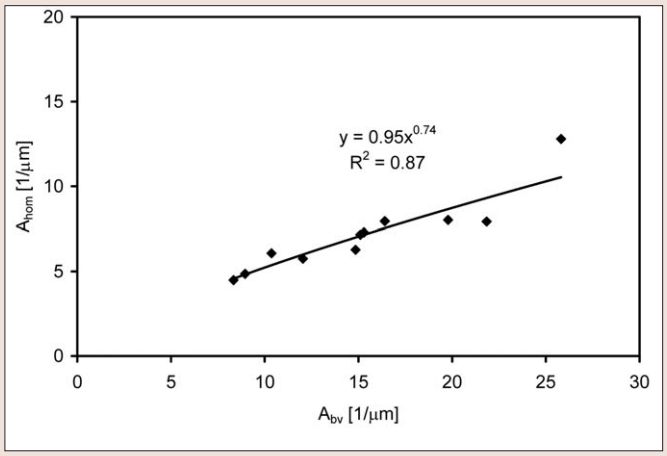


*Figure 6. Core data from well Val-3H, Tuxen Formation. Specific surface, $A_{bv}$, with respect to bulk volume as derived from BET and He-porosity data, as compared to $A_{hom}$ as calculated from porosity and permeability data by applying Kozeny's equation as formulated in Mortensen et al.*

The pseudo water film thickness, pwft, is the water saturation normalized to specific surface of pores. In the present clay-bearing formations we subtract the clay-bound water from the water saturation before normalizing:

$$\text{pwft} = (S_w - A\,\rho_g\,(1-\phi)\,/\,\phi\,X_H)\,\phi/A_{bv} \quad (8)$$

For logging data, A was derived from the GR data (equation A5); for core data A was calculated from porosity and permeability data (equations 4-7). $X_H$ is the thickness of the clay-bound water (see equations A2 and A3)

In clay-poor Maastrichtian chalk, Larsen and Fabricius found pwft to have a gradient with depth above the transition zone controlled by capillary pressure. In the more impure Danian chalk, a gradient was less easy to define. In the present case, clay content varies considerably, so a pwft gradient is difficult to establish from logging data. To overcome the problem we use Hg-air capillary pressure data from special core analysis, and recalculate them to a height above

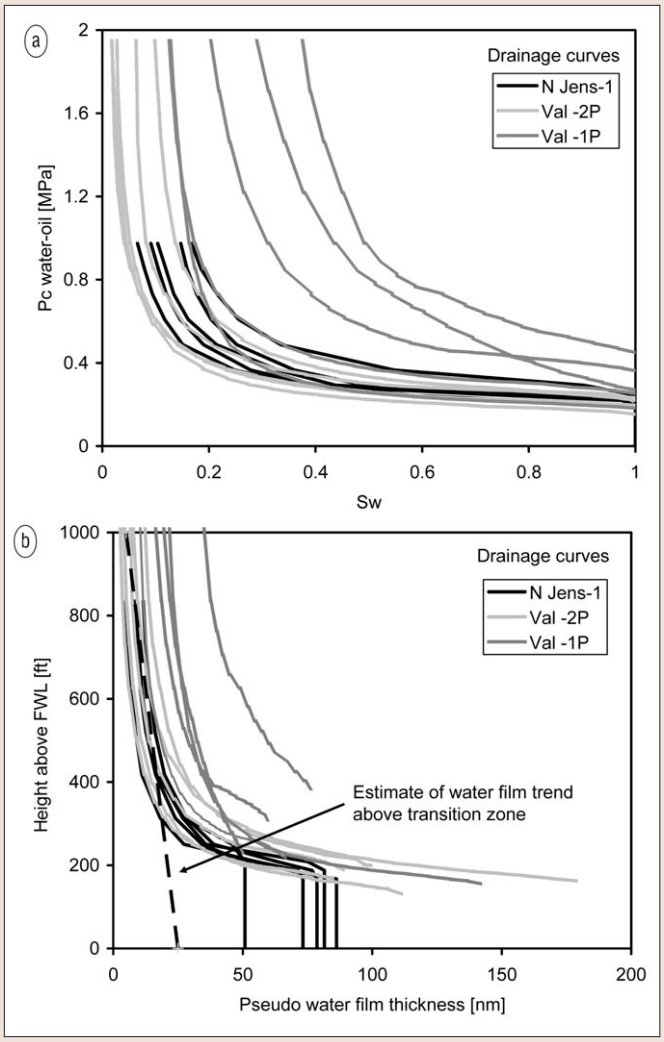


***Figure 7.*** *Capillary pressure curves calculated from gas-Hg-data (gm). (a) Capillary pressure of water-oil (bo): Pc(wo) = Pc(gm) *(σ cos Θ)wo / (σ cos Θ)gm = Pc(gm) (30*cos30/(480*cos140)) = Pc(gm)/14.15 (Archer and Wall, 1986). (b) Capillary pressure (in MPa) recalculated to ft above FWL: Height = Pc/($\rho_w$-$\rho_o$)/9.82/0.3048/1000, where $\rho_o$ = 0.64 and $\rho_w$ = 1.03. Water saturation, $S_w$, is recalculated to pseudo water film thickness, by first Klinkenberg correcting air-permeability by using the equation in Mortensen et al. and then calculating pseudofilm thickness according to Larsen and Fabricius: Film thickness = $S_w$ * ((0.52*$k^{1.083}$*9.869*$10^{-16}$)/(0.23*$\phi$))$^{1/2}$ *109 nm, where k is permeability in mD and $\phi$ is porosity. On the basis of this plot we estimate the water film trend for reservoir intervals, i.e., from samples with generally low pseudo water film thickness above the transition zone. We obtain a pseudo water film thickness of 25 nm at FWL and a gradient of 2 nm/100 ft.*

free water level versus pwft in a reservoir oil-brine system (Figure 7). We may now for relatively pure reservoir intervals predict a pwft gradient of 2 nm/100 ft and a projected film thickness of around 25 nm at the free water level. When applying capillary drainage curves from core analysis to log-interpretation, we assume that the oil column in the field is also in drainage equilibrium.

The solid particles constituting a sediment may form a more-or-less efficient supporting structure. In the case of well-cemented sediments, particles may form a stiff frame but, in newly deposited ooze, particles are close to being in suspension. In the interval between these extremes, the sediment particles are to some extent in a firm frame. The extent to which the solid phase is load-bearing may be modeled by including information from the sonic log. We use the iso-frame model of Fabricius which is based on Modified Upper Hashin Shtrikman (MUHS) bounds for the P-wave modulus, M (Figure 8):

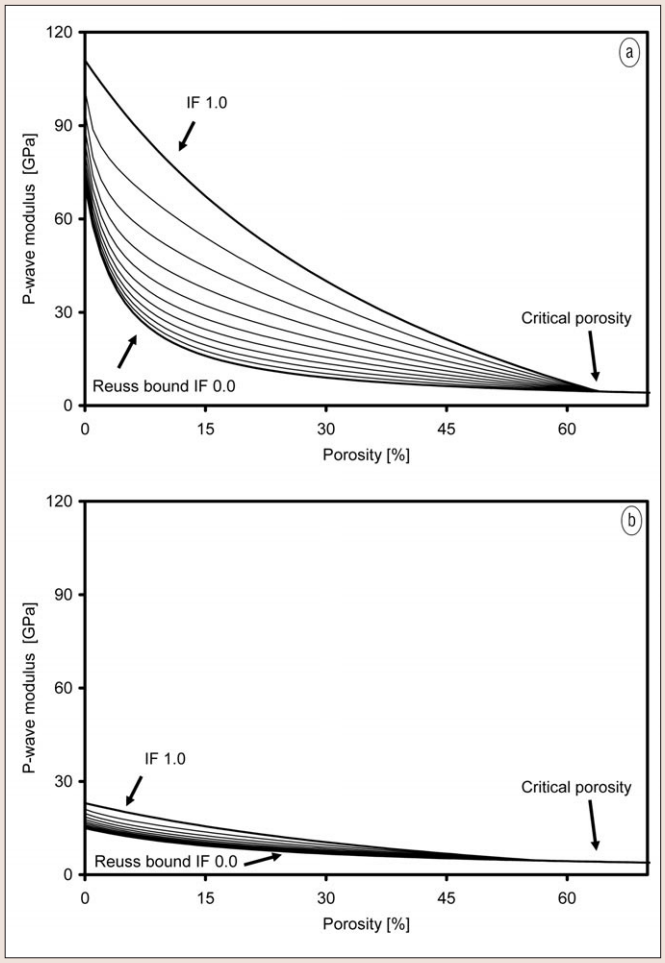


***Figure 8.*** *Modified Hashin-Shtrikman bounds for P-wave modulus of mineral-water mixtures, by assuming a critical porosity of 66%. The curves are iso-frame curves representing constant proportions of the solid in the supporting frame. The uppermost curve, IF=1.0, represents all solid in the frame and is equivalent to a modified Upper Hashin-Shtrikman bound as described by Nur et al. The lowermost curve, IF = 0.0, represents a suspension (no solid in the frame) and is equivalent to a lower Hashin-Shtrikman or Reuss bound. The position of the curves depends on mineralogy: (a) represents a calcite water system, that has relatively high moduli and (b) represents a shale-water system, that has relatively low moduli.*

$$M = \rho_b \, V_P^2 \tag{9}$$

where $V_P$ is P-wave velocity derived as the inverse of sonic transit time $\Delta_t$:

$$V_P = 1/\,\Delta_t \tag{10}$$

Intervals with high iso-frame value will be relatively stiff for a given porosity. The step-by-step procedure for calculating iso-frame value is given in Appendix 2.

**Results and discussion.** The outlined strategy for analysis of well logs differs from conventional log analysis by splitting the solid phase into load-bearing material in the frame and material in suspension, as indicated by different coloring in Figure 9. It should be stressed that the results reflect an effective medium model and not necessarily physical reality. The advantage of the procedure is that potentially weak and potentially stiff intervals may be indicated, which may give a hint on the tendency to compact.

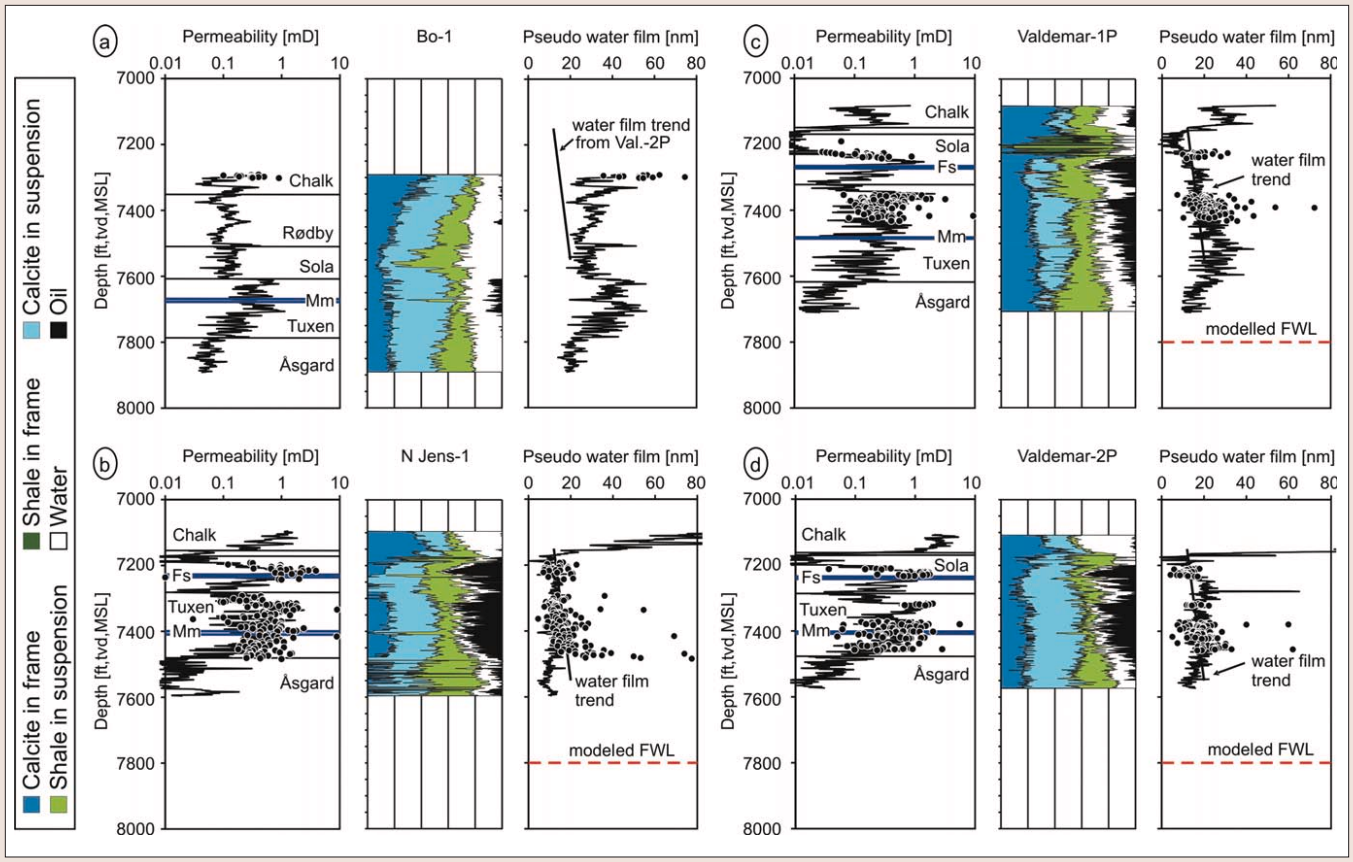


***Figure 9.*** *Permeability, composition and water film model for the wells Bo-1 (a), NJens-1 (b), Val-1P (c), and Val-2P (d). Fs = Fisch schiefer, Mm = Munk marl. Permeability was calculated from logging data by first estimating IR from the GR-log (Figure 5), then estimating specific surface from IR by using the relationship in Figure A1, then recalculating specific surface per gram to specific surface per bulk volume, $A_{bv}$, then find $A_{hom}$ by using the equation in Figure 6, and finally calculating permeability from Kozeny's equation. Where core permeability data are available the match is good. The composition of the reservoir around each well was calculated in two steps: First, shale content, porosity and water saturation were calculated by the dual water method; second, the proportion of solid in the supporting frame was calculated using the IF-model (see text). The pseudo water film thickness, pwft, for core data were calculated according to Larsen and Fabricius based on porosity, water saturation, and $A_{bv}$. For logging data, pwft is based on specific surface modeled from the GR log. It compares well with pwft derived from core data. In accordance with capillary data, a gradient of 2 nm/100 ft was visualized through reservoir (high permeability) intervals, and a FWL predicted, where a pseudo water film thickness of 25 nm (Figure 7) is indicated by extension of the straight lines.*

It appears that the lower part of Sola Formation may be relatively soft, and that the formation stiffens upwards to the extremely stiff upper part, where the silicates apparently enter the load-bearing frame. This stiff interval seems to be missing in Bo-1. The interval separating the oil-rich intervals of the Tuxen and Sola formations seems relatively soft. Åsgard Formation seems to have stiffness comparable to that of Tuxen.

Permeability predicted from logging data compares well with core data. The stiff interval in the upper part of Sola Formation apparently has very low permeability and appears to be sealing, as also indicated from the distribution of hydrocarbons. The interval separating the oil-rich intervals of Tuxen and Sola formations seem to have relatively low permeability. In most wells, Åsgard Formation appears to have intervals with very low permeability.

The pseudo water film thickness calculated from logging data compares well with calculations based on core data. Capillary pressure data from core analysis indicate a pwft gradient of around 2 nm/100 ft in the zone of irreducible water saturation and a projected pwft of around 25 nm at the free water level (FWL). When a line with a gradient of 2 nm/100 ft is visualized through the pwft data representing the purest chalk intervals from each well, we may note the following:

1) The line defined in Val-2P is not contradicted by the data from the other oil-bearing wells NJens-1 and Val-1P.
2) The oil-bearing intervals of Tuxen and Sola formations seem to fall close to the same trend.
3) In the sealing interval in the upper Sola Formation, the pwft goes below the trend of the reservoir intervals.
4) In the low-permeability interval between the reservoir sections of Tuxen and Sola formations, pwft is similar to or higher than in the reservoir sections.
5) Below the reservoir interval the wells differ. In Val-1P pwft increases in the lower part of Tuxen Formation, indicating a transition zone to the water zone. In NJens-1 and Val-2P, an increase of pwft is not seen, indicating that the entire Tuxen Formation is above the zone of transitional water saturation.
6) The low pwft in Åsgard Formation indicates that the interval is sealing, as also indicated by the low calculated permeability.
7) A pwft of 25 nm corresponds to a FWL near 7800 ft.

These observations, based on a limited number of wells, do not support the supposed stratigraphic compartmentalization of Jakobsen et al. Further, in the limited geographic area, we do not see a clear sign of a regional gradient in hydraulic head. The inclusion of more widely distributed wells may well change this result.

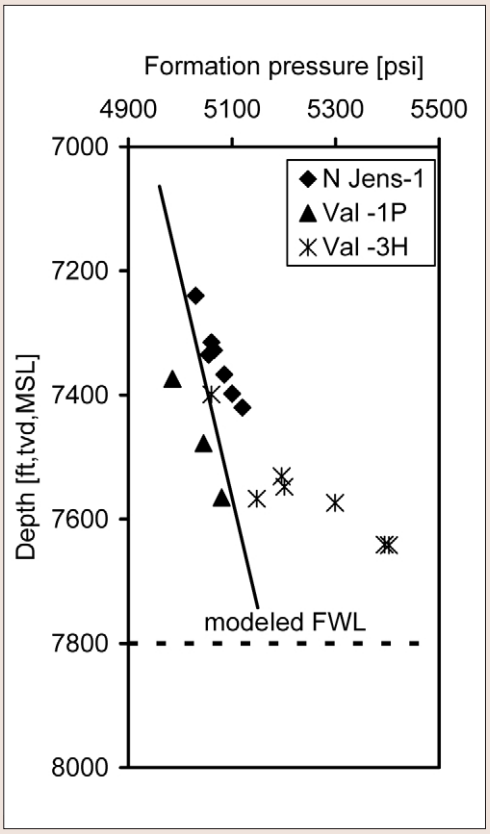


***Figure 10.*** *Wireline formation tester data (Christensen and Jakobsen, 2002) as compared to free water level as predicted from water-film model and capillary pressure data. The solid line has a gradient of 0.28 psi/ft, corresponding to a hydrocarbon density of 0.64 g/cm$^3$ from production data. If we assume that most of the data from Val-3H are influenced by supercharging, we may establish a common pressure gradient and FWL in the studied reservoir formations and wells.*

In order to address the issue of varying hydraulic head, we consulted available wireline formation tester data (Figure 10). These data are not easy to interpret, probably as a consequence of the low permeability of the reservoir intervals. Under such conditions insufficient time for equilibration may cause pressure readings that are too low; on the other hand, supercharging may lead to pressure readings that are too high. If we assume a pressure gradient equivalent to the hydrocarbon density, we may estimate a formation pressure of 34 MPa at a depth of 7400 ft, but we see no clear indication of regional gradient in hydraulic head.

**Conclusions.** Iso-frame modeling of logging data allows information from the sonic log to be directly incorporated into log analysis and, as a result, allows us to interpret relative stiffness of a sequence of sediments. Stiff layers will tend to have relatively high iso-frame value.

Pseudo water film thickness calculation allows us to normalize the water saturation to the area of the pore walls and allows us to identify zone of irreducible water saturation, transition zone, and sealing formations. Pseudo water film thickness in combination with capillary pressure core data allows us to predict the location of the free water level and to address the issue of continuity of hydraulic head between formations and regionally.

For the studied sequence of marly chalk and calcareous shale (in the North Sea, Lower Cretaceous, Cromer Knoll Group), we can formulate the following observations and conclusions:

- Åsgard Formation is variable with respect to iso-frame value and permeability, but pseudo water film thickness indicates that it is sealing with respect to hydrocarbons.
- The oil-bearing Tuxen Formation is relatively homogeneous with porosity around 30% and permeability varying generally between 0.1 and 1 mD. Iso-frame value tends to decrease upwards in a homogeneous trend from Åsgard Formation.
- A zone with relatively low permeability separates Tuxen Formation from Sola Formation. The zone has relatively low iso-frame value, and a relatively high pseudo water film thickness indicates that it is not sealing.
- The reservoir properties in the oil-bearing Sola Formation vary more than in Tuxen Formation, but the porosity may exceed 40% and the permeability may exceed 1 mD. A homogeneous pseudo water film thickness indicates hydraulic continuity with Tuxen Formation. The oil-bearing part of Sola Formation has a relatively low iso-frame value and seems to be much softer than the upper part of Sola Formation. This interval has high iso-frame value and sealing properties as indicated by low water film thickness and low permeability.

**Suggested reading.** "Incorporating capillary pressure, pore throat aperture radii, height above free-water table, and Winland r35 values on Pickett plots" by Aguilera (*AAPG Bulletin*, 2002). "Improved oil recovery and productivity from Lower Cretaceous carbonates. Combined geological/geomechanical model of the Lower Cretaceous, deformation of the horizontal boreholes" by Christensen and Jakobsen (EFP97 project, *ENS Journal No. 1313/97-0008*, Danish Energy Agency, 2002). "How burial diagenesis of chalk sediments controls sonic velocity and porosity" by Fabricius (*AAPG Bulletin*, 2003). "Characterization and zonation of a marly chalk reservoir: the Lower Cretaceous Valdemar Field of the Danish Central Graben" by Jakobsen et al. (*Petroleum Geoscience*, 2004). "Interpretation of water saturation above the transitional zone in chalk reservoirs" by Larsen and Fabricius (*SPE Reservoir Evaluation & Engineering*, 2004). "The relation among porosity, permeability, and specific surface of chalk from Gorm Field, Danish North Sea" by Mortensen et al. (*SPE Reservoir Evaluation & Engineering*, 1998). "Critical porosity: a key to relating physical properties to porosity in rocks" by Nur et al. (*TLE*, 1998). Schlumberger 1995 Log Interpretation Charts. "Resistivity index measurement without the porous plate: a desaturation technique based on evaporation produces uniform water saturation profiles and more reliable results for tight North Sea Chalk" by Springer et al. (presented at 2003 International Symposium of the Society of Core Analysts). TLE

*Acknowledgments: We thank Mærsk Oil and Gas AS for data and detailed discussions with Mærsk Oil and Gas AS personnel. We thank GEUS for data and discussions with F. Jakobsen and L. Kristensen. We also had fruitful discussions with our colleague U. Korsbech of DTU and graduate students S. Bilal and A. Shahzad. Technical assistance was provided by H. Diaz, S.H. Nguyen, and F. Kragh.*

*Corresponding author: ilf@er.dtu.dk*

## Appendix 1. Calculation of porosity and water saturation

According to Clavier et al. (1977) the dual water method may be used when pore water salinity is above 0.4 mol/l. The salinity of the pore water in the studied wells is 22 000 ppm NaCl equivalent, corresponding to 0.38 mol/l. We are thus just at the limit of the spectrum within which the dual water method can be used. At the reservoir temperature of 81° C this salinity corresponds to a water resistivity, $R_w$ of 0.12 Ωm or a water conductivity of $C_w$ of 8.33 S/m. For water-wet systems the dual water method predicts the water saturation, $S_w$ from:

$$C_t = \frac{1}{F_o} S_w^n \left[ C_w + v_Q \frac{Q_v}{S_w} (C_{cw} - C_w) \right] \quad \text{(A1)}$$

where $C_t = 1/R_t$ as given from the deep resistivity log.

The formation factor, $F_o$ may be derived from porosity: $F_o = 1/\phi^m$.

$v_Q$ is volume taken up by each charge in the clay-bound water:

$$v_Q = v X_H \quad \text{(A2)}$$

where $v$ is surface area taken up by each charge, which according to the data of Pachett as cited in Clavier et al. is equal to 450 $m^2$/meq, and $X_H$ is the thickness of the clay bound water layer, which for sodium ions at 80° C is close to 4.78 Å. $v_Q$ thus becomes 0.215 $cm^3$/meq.

$Q_v$ is charge in clay-bound water relative to pore volume:

$$Q_v = A\,(1-\phi)\rho_g / v\phi = A\,(1-\phi)\rho_g\, X_H / v_Q \phi \quad \text{(A3)}$$

where A is specific surface with respect to solid mass.

$C_{cw}$ is the conductivity of the clay-bound water, which in a Na dominated solution with salinity above 0.4 mol/l only depends on temperature. At 80° C we get $C_{cw}$ = 32.6 S/m as calculated from the relationship:

$$C_{cw} = \beta \,/\, v_Q \quad \text{(A4)}$$

where $\beta$ at 80° C may be chosen to be 7 (S/m)/(meq/$cm^3$).

A can be measured on core samples by nitrogen adsorption (BET) and is for the present samples related to IR by the equation (Figure A1):

$$A = (29.49\ IR - 1.99)\ m^2/g \quad \text{(A5)}$$

Under the assumption of a simple relationship between silicate content and GR log, A can thus be calculated from GR and density logging data (equation 3). We obtain:

$$C_t = \phi^m S_w^n \left[ C_w + \frac{A(1-\phi)\rho_g * X_H}{\phi S_w} (C_{cw} - C_w) \right] \quad \text{(A6a)}$$

$$\phi = \frac{\rho_b - \rho_g}{\rho_w S_w + \rho_o (1 - S_w) - \rho_g} \quad \text{(A6b)}$$

where $\rho_w$ and $\rho_o$ are density of formation water respectively hydrocarbons (Table 3). The petrophysical parameters m and n were for simplicity both chosen to be 1.88. A value of 1.88 for m is as predicted from $Q_v$ and $\phi$ in accordance with Clavier et al., a value of 1.88 for n does not contradict the data presented by Springer et al. (2003). In order to obtain porosity and water saturation, iteration between equations A6a and A6b has to be done, e.g. by first choosing an arbitrary value of $\phi$, then calculate $S_w$ from A6a, then calculate a new $\phi$ from A6b, and so repeating the procedure until $\phi$ and $S_w$ are stable.

**Appendix 2. Calculation of iso-frame value**

The first step is to estimate a critical porosity, $\phi_c$, corresponding to the sediment porosity at sea bottom. From a $\Delta_t$ versus $\phi$ plot, $\phi_c$ was estimated to be around 0.66 for the studied sediments of the Cromer Knoll Group (Figure A2). Data from the Chalk Group indicate a higher $\phi_c$, but as the focus on this study is on the Cromer Knoll Group, we for simplicity keep a single $\phi_c$ for all calculations.

Input data for the iso-frame modeling are the following data from logs: porosity, $\phi$, volume of insoluble residue, $IR_{bv}$,

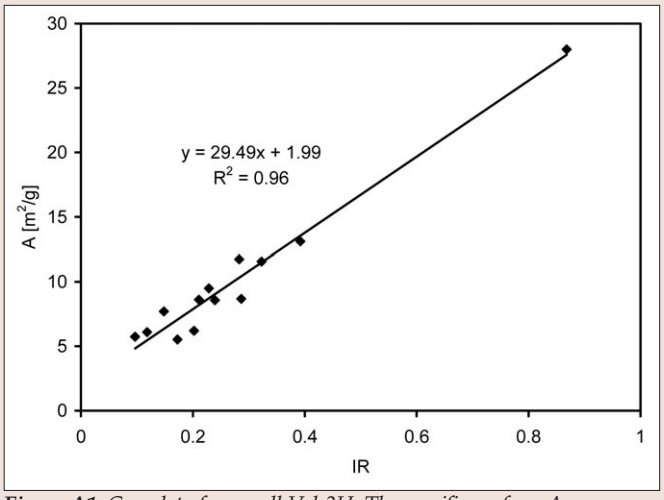


***Figure A1.*** *Core data from well Val-3H. The specific surface, A, as measured by nitrogen adsorption (BET) correlates well with insoluble residue, IR, as measured by wet chemical analysis.*

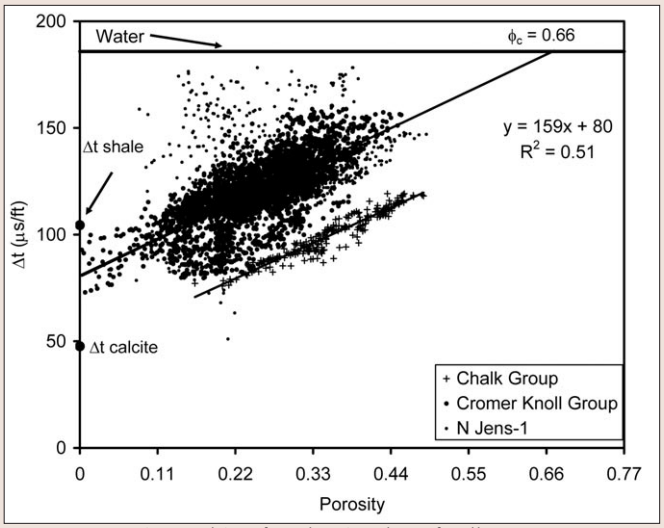


***Figure A2.*** *Sonic traveltime from logging data of wells Bo-1, NJens-1, Val-1P, and Val-2P have distinct porosity trends for the Chalk Group interval and the Cromer Knoll Group interval. The Cromer Knoll Group data define a trend-line which reaches the velocity of the pore water at a critical porosity, ϕc, of 0.66. Data from NJens-1 are noisy and were left out of the correlation.*

water saturation, $S_w$, and P-wave modulus, M; as well as $\phi_c$ and elastic data for calcite, insoluble residue ("shale"), hydrocarbons and water (Table 3). Volume of calcite, $C_{bv}$ is:

$$C_{bv} = 1 - IR_{bv} - \phi \quad \text{(A7)}$$

The second step is to calculate the bulk modules, $K_{fl}$, of the pore fluid in the zone investigated by the sonic log. In the exploration wells, Bo-1 and NJens-1 for simplicity full invasion was assumed, so that all hydrocarbons are displaced and the pore fluid was assumed to be similar to that of formation water. In the pilot holes, Val-1P and Val-2P, a situation of no invasion was assumed, and $S_w$ was assumed near irreducible, so that water supports the pores, and water and oil should be mixed according to the "stiff" Voigt average:

$$K_{fl} = S_w\, K_w + (1-S_w)\, K_o \quad \text{(A8)}$$

***Table 3.*** *Data used for log interpretation and modeling*

| Wireline logs | Reservoir data | Fluid properties at reservoir conditions | | Mineral properties | |
|---|---|---|---|---|---|
| | | Oil | Water and aqueous mud filtrate | Calcite | "Shale" |
| Caliper | Temp.: 81° C at 7300 ft ss | Density , $\rho_o$ = 0.64 g/cm$^3$ | Density, $\rho_w$ = 1.03 g/cm$^3$ | Grain density, $\rho_g$ = 2.7 g/cm$^3$ (Ref. Figure 3) | Grain density, $\rho_g$ = 2.7 g/cm$^3$ (Ref. Figure 3) |
| NGR | Initial reservoir pressure: 5000 psia at 7200 ft ss | P-wave velocity*, $V_P$ = 1132 m/s | P-wave velocity, $V_P$ = 1640 m/s | P-wave velocity, $V_P$ = 6400 m/s | P-wave velocity, $V_P$ = 2919 m/s |
| Density | | Bulk modulus, $K_o$ = 0.82 GPa | Bulk modulus, $K_w$ = 2.77 GPa | Bulk modulus $K_c$ = 71 GPa | Bulk modulus $K_s$ = 15 GPa |
| Neutron | | | | Shear modulus, $G_c$ = 30 GPa | Shear modulus, $G_s$ = 6 GPa |
| Borehole corrected sonic | | | Salinity: 22 000 ppm (NaCl equivalent) | P-wave modulus, $M_c$ = 111 GPa | P-wave modulus, $M_s$ = 23 GPa |
| Deep and shallow resistivity | | | Resistivity** $R_w$ = 0.12 Ωm Conductivity $C_w$ = 8.33 S/m | | |

**P-wave velocity of oil was calculated from density, temperature and pressure from the "dead oil" equation in Mavko et al. (1998):

$V_P$(m/s) = 2096 $[\rho_o/(2.6-\rho_o)]^{1/2}$ - 3.7t +4.64P +0.0115 $[4.12\ (1.08\rho_o^{-1} -1)^{1/2} -1]$tP, where t is temperature in °C, and P is pressure in MPa. We assume $\rho_o$ = 0.64. Bulk modulus of fluids were calculated from K = M = $\rho\ V_P^2$. Elastic moduli of solids were chosen based on citations in Mavko et al. (1998).

** Resistivity was read from Schlumberger (1995).

where $K_w$ is bulk modulus of water and $K_o$ is bulk modulus of oil (Table 3).

The third step is to assume arbitrary start-out iso-frame values for "shale" $IF_s$ and calcite, $IF_c$ indicating to which extent the two components are load-bearing. During modeling, $IF_s$ and $IF_c$ are adjusted until the measured M is correctly predicted. In accordance with petrographic data we assume a start-out $IF_s$ of 0, and during modeling only let $IF_s$ grow when $IF_c$ has reached 1.

The fourth step is to calculate bulk modulus, $K_{sus}$ of the suspension of pore fluids and solids not in the frame. This was done by a Reuss model:

$$K_{sus} = \frac{1}{(1-IF_c)C_{bv}/K_c + (1-IF_s)IR_{bv}/K_s + \phi/K_{fl}}$$

where $K_c$ and $K_s$ are bulk moduli of calcite respectively shale (Table 3).

The fifth step is to normalize proportion of suspension and solids (calcite and "shale") in frame to critical porosity:

$$sus_c = \phi/\phi_c + ((1 - IF_c)C_{bv} + (1 - IF_s)IR_{bv})\ (1 - \phi/\phi_c)/(1 - \phi) \quad (A10)$$

$$C_c = IF_cC_{bv}(1 - \phi/\phi_c)/(1 - \phi) \quad (A11)$$

$$IR_c = IF_sIR_{bv}(1 - \phi/\phi_c)/(1 - \phi) \quad (A12)$$

The sixth step is to calculate the MUHS bound for the bulk modulus, $K_{HS+}$ based on the formulation of Berryman as cited in Mavko et al. (1998):

$$K_{HS+} = 1/(C_c/(K_c + 4/3G_c) + (IR_c/(K_s + 4/3G_c) + sus_c/(K_{sus} + 4/3G_c)) - 4/3G_c \quad (A13)$$

where $G_c$ is the shear modulus of calcite (Table 3).

The seventh step is to calculate the MUHS bound for the shear modulus $G_{HS+}$ based on the formulation of Berryman as cited in Mavko et al.:

$$G_{HS+} = 1/(C_c/(G_c + \zeta) + IR_c/(G_s + \zeta) + sus_c/\zeta) - \zeta \quad (A14)$$

where $\zeta = G_c/6\ ((9K_c + 8G_c)/((K_c + 2G_c)))$

The eighth step is to calculate P-wave modulus:

$$M_{HS+} = K_{HS+} + \tfrac{4}{3}\ G_{HS+} \quad (A15)$$

$M_{HS+}$ should now be compared with M from logging data (equation 9) and IFs adjusted until an acceptable fit is found. In the present case IFs were adjusted to the closest decimal.